The Mechanism of Emerging Catalytic Activity of Gold Nano-clusters on Rutile TiO$_2$(110) in CO Oxidation Reaction

K. Mitsuhara[1], M. Tagami[1], T. Matsuda[1], A. Visikovskiy[1*], M. Takizawa[2], and Y. Kido[1]

1) Department of Physics, Ritsumeikan University, Kusatsu, Shiga-ken 525-8577, Japan
2) SR Center, Ritsumeikan University, Kusatsu, Shiga-ken 525-8577, Japan

Abstract

This paper reveals the fact that the O adatoms (O$_{ad}$) adsorbed on the 5-fold Ti rows of rutile TiO$_2$(110) react with CO to form CO$_2$ at room temperature and the oxidation reaction is pronouncedly enhanced by Au nano-clusters deposited on the above O-rich TiO$_2$(110) surfaces. The optimum activity is obtained for 2D clusters with a lateral size of ~1.5 nm and two-atomic layer height corresponding to ~50 Au atoms/cluster. This strong activity emerging is attributed to an electronic charge transfer from Au clusters to O-rich TiO$_2$(110) supports observed clearly by work function measurement, which results in an interface dipole. The interface dipoles lower the potential barrier for dissociative O$_2$ adsorption on the surface and also enhance the reaction of CO with the O$_{ad}$ atoms to form CO$_2$ owing to the electric field of the interface dipoles which generate an attractive force upon polar CO molecules and thus prolong the duration time on the Au nano-clusters. This electric field is screened by the valence electrons of Au clusters except near the perimeter interfaces, thereby the activity is diminished for three-dimensional clusters with a larger size.

* Present address: *Department of Applied Quantum Physics and Nuclear Engineering, Kyushu University, 744 Motooka Nishi-ku, Fukuoka 819-0395, Japan*

I. INTRODUCTION

As well known, the rutile $TiO_2(110)$ has been utilized as a support of metal clusters for real and model catalysts. Haruta[1] found a strong catalytic activity of Au nano-clusters dispersed on the rutile TiO_2 particles even at low temperatures for the size below ~5 nm. Up to now, many efforts have been made experimentally and also theoretically to elucidate the mechanism of emerging catalytic activity of Au nano-clusters in CO oxidation reaction[2-9]. There are three candidates to explain the emerging catalytic activity; (i) simple geometrical effect, (ii) quantum size effect, and (iii) electronic charge transfer between Au nano-clusters and supports. As another possibility, OH (hydroxyl) may play an important role in a process like water gas shift reaction ($H_2O + CO \rightarrow CO_2 + H_2$)[10,11]. The geometrical effect (i) means that the active site is the perimeter interface between Au nano-clusters and supports and thus the reaction rate per constituent Au atom is proportional to $1/d^2$, where d is an average diameter of Au clusters (partial spheres are assumed). Such a behavior was recently reported by Fujitani and Nakamura[12] for Au-supported rutile $TiO_2(110)$ at high pressures of a mixed CO and O_2 gas containing H_2O. As the quantum size effect, the drastic change of the d-band width and d-band center starts from the size below ~100 Au atoms/cluster[13]. However, the d-band center moves apart from the Fermi level (E_F) with decreasing the cluster size due to a strain effect[13], indicating inapplicability of the d-band model[14] to explain the emerging catalytic activity of Au nano-clusters. It was theoretically demonstrated that an electronic charge transfer takes place from Au clusters to O-rich $TiO_2(110)$ supports and the CO oxidation reaction is pronouncedly enhanced[6,9].

In the previous study, we found a reaction path of CO oxidation on O-rich rutile $TiO_2(110)$ surfaces[15], which were prepared by exposing reduced (R)-TiO_2 surfaces to O_2 at almost room temperature (RT). The O-rich surface denoted by O-$TiO_2(110)$ has unfilled bridging O vacancies (V_O) and O adatoms on the 5-fold Ti rows and the latter reacts with CO molecules to form CO_2[15,16]. Figure 1 illustrates the O-$TiO_2(110)$ surface with a ball and stick model. The above fact was revealed by high-resolution medium energy ion scattering (MEIS) combined with photoelectrons spectroscopy (PES) using synchrotron-radiation (SR) light[15,16]. The O deficiency and excess on the surfaces are evaluated quantitatively by detecting the Ti 3d defect state (Ti^{3+} state) intensity in ultraviolet photoelectron spectra (UPS), because O is an electronegative

species and thus O adsorption and desorption accompany electronic charge transfer via exchange of $Ti^{3+} \leftrightarrow Ti^{4+}$[17-20].   The adsorbed O is assigned by isotopically labeled ^{18}O, which is detected by MEIS separately from ^{16}O[15,16].
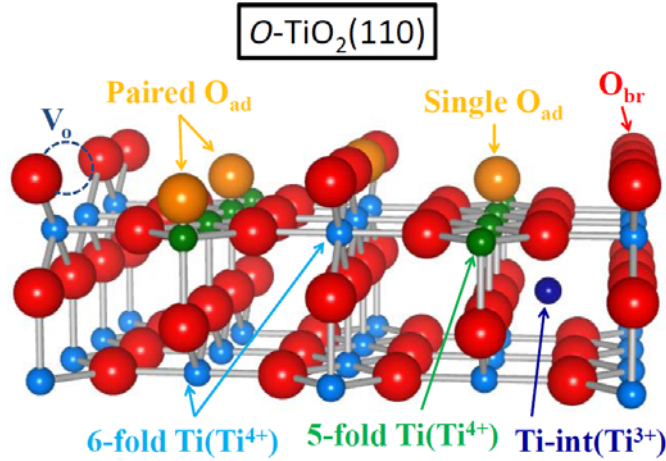

Fig. 1. Ball and stick model for O-TiO$_2$(110).   Orange balls represent O$_{ad}$ atoms and V$_O$ is bridging O vacancy. Small dark-blue ball denote Ti interstitial acting as an n-type donor.

In this study, we demonstrate a pronounced enhancement of the CO oxidation reaction by Au nano-clusters deposited on the rutile TiO$_2$(110) surfaces.   The mechanism of the emerging catalytic activity of Au nano-clusters is elucidated in terms of electronic charge transfer between Au nano-clusters and the support, which is evaluated quantitatively by binding energy shifts of O 2s, Ti 3p, and valence band edge as well as work function measurements.   The activity of Au nano-clusters depends strongly on the size and shape, which are determined by high-resolution MEIS[21]. All the experiments were performed *in situ* under ultra-high vacuum (UHV) conditions ($< 2 \times 10^{-10}$ Torr).

II. EXPERIMENT

As-supplied TiO$_2$(110) surfaces were annealed at 980 K for 30 min in UHV after sputtering with 0.75 keV Ar$^+$ ions.   As a result, the specimens changed the color from transparency to blue due to creation of O-vacancies acting as an F-center and simultaneously became conductive (n-type semiconductor) caused by Ti-interstitials (Ti-int) as an electron donor (Ti^{3+})[22,23].   The clean (1×1) surfaces without Ti-rich oxide clusters were checked by reflection high-energy electron diffraction (RHEED)

combined with medium energy ion scattering (MEIS) analysis using 80 keV He$^+$ ions. Indeed, if such Ti-rich clusters exist on the surface, the spectra from Ti and O become broad under the scattering geometry of the [100]-incidence and [010]-emergence. We employed 80 keV He$^+$ ions for analysis of O because of the best sensitivity to such low Z-number atoms, while 120 keV He$^+$ beams were used to analyze Au nano-clusters.

We measured ultraviolet photoelectron spectra (UPS) at photon energy of 50 eV close to the resonance energy of 47 eV[24] using SR-light. Valence band spectra including the Ti 3d defect state seen ~0.8 eV below the E_F as well as O 2s and Ti 3p lines were observed at [1$\bar{1}$0] azimuth under normal emission condition. Note that observation at the [1$\bar{1}$0]-azimuth is more sensitive to the Ti 3d defect state intensity rather than the [001]-azimuth. The UPS analysis is also available to check the Ti-rich clusters, which give broad valence band spectra, clearly distinguished from those for the clean 1×1 surface. We also measured the work function by taking secondary electron emission spectra induced by 140 eV photon impact on the sample surfaces, which were negatively biased[25].

We prepared the O-TiO$_2$(110) surfaces by exposure of O$_2$ (5N) onto reduced surfaces denoted by R-TiO$_2$(110), which were formed by sputtering with 0.75 keV Ar$^+$ followed by annealing at 870 K for 10 min in UHV. The above O$_2$ exposure was carried out starting from a temperature of ~325 K and down to RT at a same O$_2$ pressure (5×10^{-6} Torr). It is difficult to prepare a perfectly stoichiometric surface, because annealing R-TiO$_2$(110) surfaces in an O$_2$ ambience causes extraction of Ti-int atoms from the bulk and near-surface region to form added-layers of TiO$_2$(110) often a partially incomplete surface structure involving Ti$_2$O$_3$-like clusters[26]. Despite that we tried to form almost a stoichiometric surface by exposing the R-TiO$_2$(110) surface to O$_2$ (1×10^{-6} Torr) at 820 K for 5 min (300 L; 1 L = 10^{-6} Torr s). The nearly stoichiometric surface was confirmed by MEIS and UPS as mentioned before.

Au nano-clusters were grown on TiO$_2$(110) at RT by molecular beam epitaxy at a deposition rate of 0.2~0.3 ML/min, where 1 ML is equal to 1.39×10^{15} atoms/cm^2, corresponding to the areal number density of Au(111). The average size and shape (two-dimensional (2D) and three-dimensional (3D)) were determined by high-resolution MEIS[21]. Here, the 2D clusters were defined by the height below two atomic layers and the 3D shape was approximated by a partial sphere with a diameter d and height h. Note that the RHEED, MEIS, and UPS analyses were made at RT and all the

experiments were performed *in situ* under UHV condition ($\leq 2 \times 10^{-10}$ Torr) at the beamline-8 named SORIS at Ritsumeikan SR Center.

III. RESULTS AND DISCUSSION

A. Growth mode of Au nano-clusters

We first analyzed the growth mode of Au nano-clusters on the O-TiO$_2$(110) by high-resolution MEIS.   Before showing the results, we briefly explain the characteristics of the MEIS analysis, which is based on the binary collision approximation. If an ion with an incident energy of E_0 is scattered by a target atom, the scattered energy is given by

$$E_1 = (\frac{\sqrt{1 - R^2 \sin^2 \theta} + R \cos \theta}{1 + R})^2 E_0 \qquad (R \equiv M_1 / M_2), \qquad (1)$$

where θ, M_1, and M_2 are scattering angle and projectile and target masses, respectively. Thus a scattering with a lighter atom results in a smaller scattered energy (E_1) allowing for a target mass analysis.   If an ion undergoes a binary elastic scattering in a solid at a depth of x, the ion loses its energy gradually via interactions with the electrons of the solid mainly valence electrons. This energy loss proportional to a path-length in the solid gives the information about the depth where the ion undergoes the large angle scattering (usually more than 10°). The scattering yield from some target atom species (j) is basically given by

$$Y_j(\theta) = Q \ (d\sigma / d\Omega)_j \Delta\Omega \ N_j \Delta x \ \varepsilon \ \eta_+, \qquad (2)$$

where $(d\sigma / d\Omega)_j$, $\Delta\Omega$, $N_j \Delta x$, and Q, respectively are scattering cross section, solid angle subtended by a detector (7.64×10^{-5} str), the number of target atoms of interest (atoms/cm^2), and the number of incident ions on the target sample measured by integrated beam current. The detection efficiency ε of the toroidal spectrometer used here is 0.44 and a He$^+$ fraction denoted by η_+ dependent on emerging energy and angle was measured in advance.   The observed MEIS spectrum is best-fitted assuming a target structure.   The MEIS spectrum is easily constructed by superimposing each scattering component from a subdivided thin slab (layered structure) or small cube (clusters)[21,27].   In the present MEIS analysis, the EMG (exponentially modified Gaussian shape) function was employed as an asymmetric line shape[28,29].

Figure 2(a) shows typical MEIS spectra observed for Au deposition of 0.19, 0.91, and 1.57 ML, respectively from the bottom to top.   The curves correspond to

best-fitted spectra assuming average diameter of 2.0 (3.1) nm and height of 1.1 (1.5) nm for the middle (top) MEIS spectrum. For Au deposition of 0.19 ML, the MEIS spectrum is deconvoluted into two components from 2D and 3D clusters, where the 2D clusters have two atomic layer height (0.235×2 nm) and areal occupation ratio of 10 %, while the 3D clusters take a shape of partial sphere with $d = 1.4$ and $h = 0.7$ nm and an areal occupation ratio of 3.5 %. Note that the height of 0.7 nm corresponds to three atomic layer height. Unfortunately, it is impossible to determine the lateral size of 2D clusters by MEIS. Figure 2(b) shows the diameter and height for 3D clusters as a function of Au coverage. Interestingly, both d and h take constant values of 1.4 and 0.7 nm, respectively up to Au coverage of 0.4 ML and then increase almost linearly with increasing Au coverage. This indicates a critical lateral size of 1.4 nm with three atomic layer height. The areal occupation ratios for 2D and 3D clusters are indicated in Fig. 2(c) as a function of Au coverage. Starting from 2D cluster formation, the number of clusters increases probably keeping the lateral size of 1.4 nm up to Au coverage of 0.4 ML, where all the 2D clusters change into 3D clusters with the above critical size. With further Au deposition the 3D clusters start to grow into a lager size taking a shape of almost hemispherical ones to lower the surface energy. Such a growth mode is different from that for R-TiO$_2$(110) substrates, where 3D cluster growth starts initially owing to the fact that bridging O vacancy (V$_O$) acts as a nucleation site[30,31].
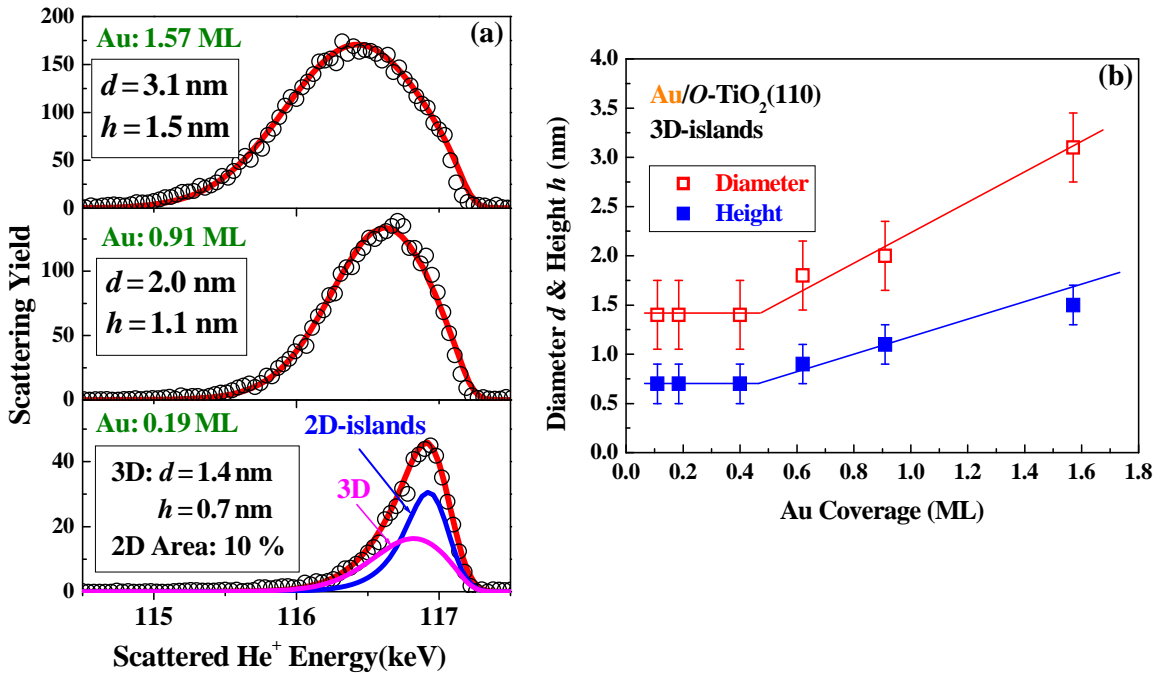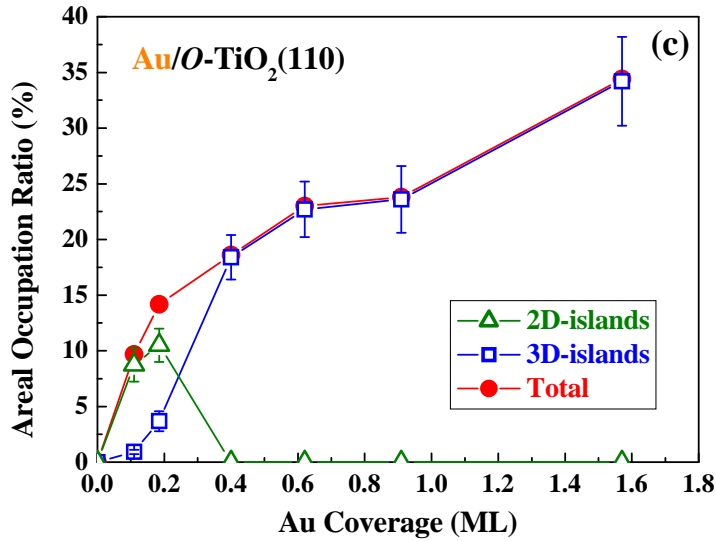
Fig. 2. (a) Typical MEIS spectra observed for 120 keV He$^+$ ions incident along [110]-axis and scattered to $[1\bar{1}0]$ direction of TiO$_2$(110) onto which Au clusters were formed with coverage of 0.19, 0.91, and 1.57 ML from the bottom to top. Solid curves are best-fit spectra assuming partial spheres for Au clusters with average diameter of 2.0 (3.1) nm and height of 1.1 (1.5) nm for Au coverage of 0.91 (1.57) ML. MEIS spectrum for Au coverage of 0.19 ML is best-fitted assuming coexistence of 3D (d = 1.4 and h = 0.7 nm) and 2D clusters with two atomic layer height and areal occupation ratio of 10 %. (b) Average diameter d (open squares) and height h (closed squares) determined by MEIS for 3D clusters as a function of Au coverage. (c) Areal occupation ratios for 2D (triangles) and 3D (squares) clusters as a function of Au coverage. Closed circles denote areal occupation ratios of 2D plus 3D clusters.

B. Reaction of CO with O$_{ad}$ atoms

Our concern is the enhancement of CO oxidation at RT mediated by Au nano-clusters. Figure 3 shows the UPS spectra taken for R- and O-TiO$_2$(110) before and after CO exposure (2×10^{-5} Torr) as well as Au(0.05 ML)/O-TiO$_2$(110) after CO exposure. Here, the CO gas with a purity of 4N was dosed at RT and we checked the partial pressures of H$_2$ and H$_2$O less than 100 ppm during CO exposure with a quadrupole mass filter. The inset indicates the magnified spectra of the gap state identified as Ti 3d defect state (Ti^{3+}), which holds an electronic excess charge. The origin of this gap state is still a debatable issue. It has been recognized that creation of a V$_O$ gives an electronic charge to underlying Ti atoms making the Ti^{4+} state into Ti^{3+} state[18,19,32]. Recently, however, Wendt et al.[17] claimed that the gap state comes from the Ti-int acting as an

electron donor condensed near the surface by annealing in UHV. Apart from the origin of the gap state, the defect state intensity observed for R-TiO$_2$(110) almost disappears after O$_2$ exposure of 1000 L at RT (more exactly from ~325 K down to RT) and then exposing the O-TiO$_2$(110) to CO at RT produces the gap state again as shown in Fig. 3.
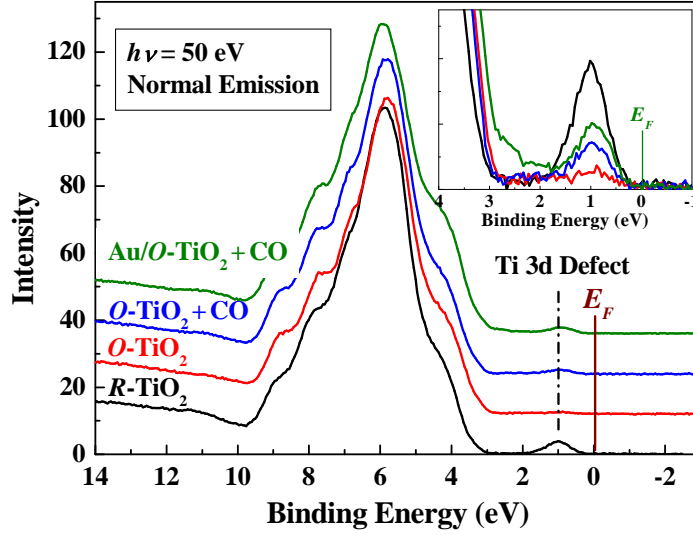

Fig. 3. UPS spectra observed at photon energy of 50 eV under normal emission condition for R-, O-TiO$_2$(110), and O-TiO$_2$(110) and Au(0.05 ML)/ O-TiO$_2$(110) after CO exposure of 12000 L. Binding energy (E_B) is scaled from Fermi level (E_F).   Inset indicates magnified spectra of Ti 3d defect state.

The defect state intensity is considerably enhanced by exposing Au(0.05 ML)/O-TiO$_2$(110) to CO.   As reported previously[15], the disappearance of the gap state for R-TiO$_2$ after O$_2$ exposure is attributed to the fact that the electronic excess charge (Ti^{3+}) is consumed to heal V$_O$ vacancies partly and to adsorb O atoms (O$_{ad}$) on the 5-fold Ti rows. Indeed, the electronic charge to create an O$_{ad}$ of electro-negative species was estimated to be *0.7 − 0.9 e* (*e*: electron charge) from the first principles calculations[17,33,34]. The appearance of the gap state after CO exposure originates from disappearance of the O$_{ad}$ atoms by reaction with CO to form CO$_2$.   The defect state intensities are normalized by the intensity for R-TiO$_2$(110) after subtracting the intensity for O-TiO$_2$(110) and shown in Fig. 4. The normalized defect state intensities for O-TiO$_2$ and Au(0.05 ML)/O-TiO$_2$, respectively are saturated to be ~0.33 and ~0.6 at CO exposure more than 12,000 L. The above results reveal that the presence of Au nano-clusters enhances pronouncedly the oxidation reaction between O$_{ad}$ and CO.

Such a trend is also observed as reduction of ^{18}O after exposing ^{18}O-TiO$_2$(110) to CO at RT and appearance of ^{18}O for O-TiO$_2$(110) after CO exposure followed by $^{18}O_2$ dose, as will be presented later. The reason why the number of O_{ad} is saturated to be ~10 % of the surface atomic density (5.2×10^{14} atoms/cm^2) and all the O_{ad} do not react with CO is due to the theoretical prediction that the increase in the coverage of O_{ad} increases the potential barrier for O adsorption on the 5-fold Ti rows[17]. The above fact that the coverage of O_{ad} is saturated at ~10 % seems reasonable, because the increase in O_{ad} of negative species leads to increase in electrostatic surface energy making the surface unstable just like a polar face of ionic crystals. It is intractable to deduce exactly the ratio of O_{ad} which reacted with CO, because the electronic excess charge is partly consumed to heal V_O and the charge required is not known. However, the ratio of the O_{ad} atoms reacted with CO was estimated roughly to be ~60 % for O-TiO$_2$ and almost 100 % for Au(0.05-0.08 ML)/O-TiO$_2$ by determining the absolute amount of adsorbed O except that healed V_O by means of MEIS combined with elastic recoil detection analysis[15,16].
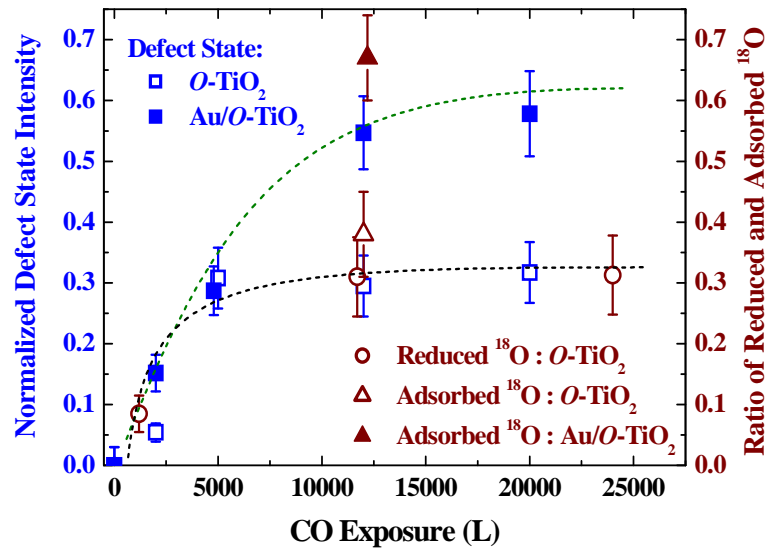

Fig. 4. The defect state intensity normalized by that for R-TiO$_2$(110) indicated for O-TiO$_2$(110) (open squares) and for Au(0.05 ML)/O-TiO$_2$(110) (closed squares) as a function of CO exposure. Right side axis: Ratio of reduced ^{18}O after CO exposure to original amount of ^{18}O before CO dose (open circles). Here, ^{18}O-TiO$_2$(110) surface was exposed to CO at RT, which was formed by exposing R-TiO$_2$(110) to $^{18}O_2$. Ratios of adsorbed ^{18}O to original amount of ^{18}O for ^{18}O-TiO$_2$(110) are indicated for O-TiO$_2$(110) (open triangle) and Au(0.08 ML)/O-TiO$_2$(110) (closed triangle). Here, ^{18}O atoms were adsorbed after CO exposure of 12000 L followed by $^{18}O_2$ dose (1000 L). Dashed curves are drawn to guide the eyes.

The absolute amounts of adsorbed O were determined by MEIS using $^{18}O_2$ (5N, 98 %) as the exposure gas. Figure 5(a) shows the MEIS spectrum observed for R-TiO$_2$(110) after exposed to $^{18}O_2$ (5×10^{-6} Torr, 1000 L) at ~325 K - RT. The inset indicates the magnified spectrum around the signal from ^{18}O. The amount of ^{18}O is deduced to be $4.6\pm0.3\times10^{13}$ atoms/cm^2, corresponding to ~8.8 % of the (110) surface atoms (5.2×10^{14} atoms/cm^2). The best-fit was performed in such a way that the simulated area for ^{18}O coincides with the observed one after subtracting background whose level was determined after 5-point smoothing. The error bars originate from reproducibility and statistics. According to scanning tunneling microscopy (STM) observations[17,33] and our previous analysis[16], the O$_2$ molecules of an exposure gas are adsorbed in the V$_O$ vacancies (almost half or less are healed) and in the 5-fold Ti rows. There are two O$_2$ dissociation channels[17,33]; (i) an O$_2$ molecule is dissociatively adsorbed in a V$_O$ site; one heals the V$_O$ and another sits on a 5-fold Ti row (single O$_{ad}$) and (ii) an O$_2$ molecule is adsorbed dissociatively on a 5-fold Ti atom (paired O$_{ad}$). Correlating with the Ti 3d defect state intensity appearing after CO exposure (see Figs. 3), the amounts of ^{18}O for the ^{18}O-TiO$_2$(110) formed by exposing R-TiO$_2$(110) to $^{18}O_2$ are reduced by CO dose via reaction between CO and O$_{ad}$[15]. The reduction ratio normalized by the amount of ^{18}O adsorbed on the R-TiO$_2$(110) (^{18}O-TiO$_2$) is indicated by the open circles in Fig. 4. The reduction ratios for ^{18}O measured by MEIS are quite consistent with the UPS result.
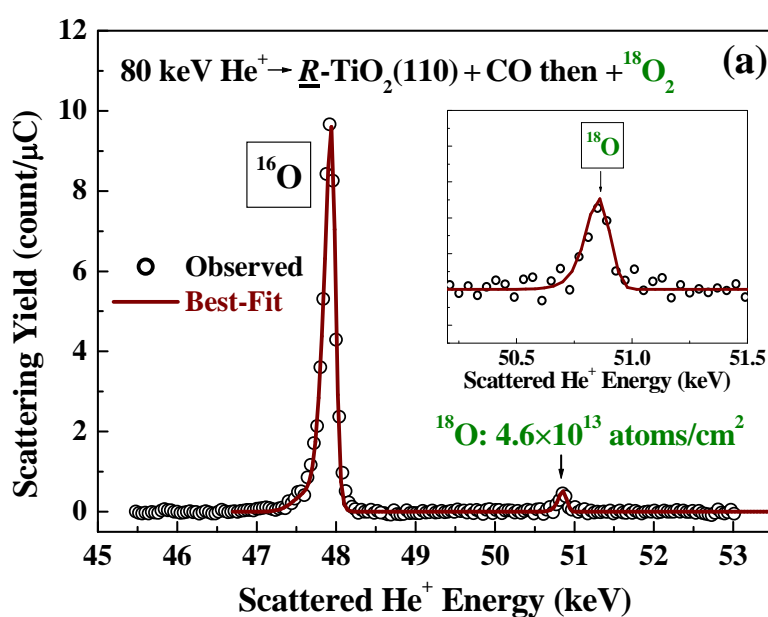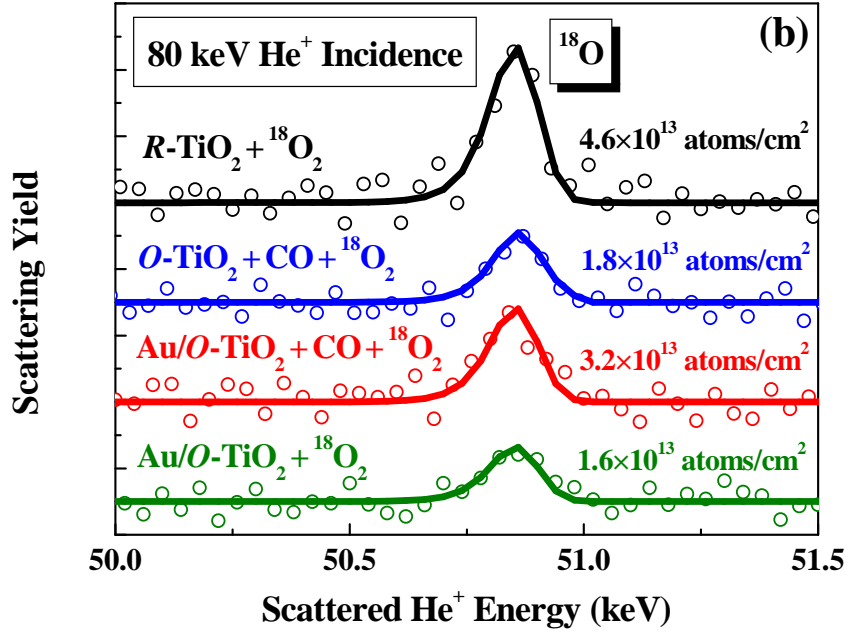
Fig. 5. (a) MEIS spectrum measured for 80 keV He$^+$ ions incident along the [100]-axis and backscattered from ^{16}O and ^{18}O to the [010] direction of R-TiO$_2$(110) after CO exposure of 12000 L followed by $^{18}O_2$ dose (1000 L) at RT   Solid curve is the best-fitted spectrum assuming the amount of 4.6×10^{13} atoms/cm^2 for adsorbed ^{18}O atoms.   Inset is magnified spectrum around the scattering component from ^{18}O. (b) Magnified MEIS spectra around the scattering component from ^{18}O indicated for R-TiO$_2$ after $^{18}O_2$ exposure (1000 L), O-TiO$_2$ and Au(0.08 ML)/O-TiO$_2$ after CO exposure (12000 L) followed by $^{18}O_2$ dose, and Au(0.08 ML)/O-TiO$_2$ after $^{18}O_2$ dose (1000 L) at RT.   Solid curves are best-fitted spectra assuming each amount of ^{18}O to be 4.6, 1.8, 3.2, and 1.6×10^{13} atoms/cm^2 with uncertainty of $\pm0.3\times10^{13}$ atoms/cm^2 from the top to bottom spectrum.

Recently Zhao et al.[35] and Wang et al.[36] observed CO adsorption on the 5-fold Ti rows and migration on R-and O-TiO$_2$(110) surfaces by STM and estimated the adsorption energy and diffusion barrier along the 5-fold Ti rows to be 0.38 and 0.32 - 0.35 eV, respectively based on the first principles calculations. Here, if we assume a simple model that a CO molecule diffuses along the 5-fold Ti row leading to encounter with an O$_{ad}$ atom, which results in CO oxidation with an activation barrier of E_a.   In the case of CO adsorbed on the O-TiO$_2$(110), the number of reacted O$_{ad}$ atoms N_{ad} (atoms/cm^2) after CO exposure of x [L] is given by

$$N_{ad} \cong 4 \times 10^{14} \ x \ exp[-E_a / k_B T] \ , \hspace{3cm} (3)$$

where k_B and T are Boltzmann constant and temperature, respectively. If we put the values of $N_{ad} \cong 2 \times 10^{13}$ atoms/cm^2, x = 12000 L, and $k_B T = 0.025$ eV (RT), the E_a value of 0.31 eV is deduced. The enhanced N_{ad} about twice by the presence of Au nano-clusters leads to a slight reduction of E_a (0.29 eV). We must note that this estimate is quite rough. In order to derive the E_a value exactly, the oxidation rate should be measured using a quadrupole mass filter, for example.

Here, some attention should be paid to the effect of H_2O unintentionally involved in the CO gas. According to Du et al.[37], a water molecule adsorption on O-TiO$_2$(110) surface at RT creates an $O_{ad}H$ pair on the 5-fold Ti row and an immediate recombination results in formation of a new water molecule, leaving behind an O_{ad} that comes from the original H_2O. This process may lead to reduction of ^{18}O during CO exposure. In order to check this process, we prepared ^{18}O-TiO$_2$(110) and measured the amounts of ^{18}O before and after $H_2^{16}O$ exposure of 1 L (1×10^{-8} Torr for 100 sec). As the result, we found only a slight reduction of ^{18}O within an experimental uncertainty after the H_2O exposure ($4.3\pm0.3\times10^{13}$ atoms/cm^2 → $4.0\pm0.3\times10^{13}$ atoms/cm^2). Therefore, it is reasonable to make interpretation that the reduction of ^{18}O after CO exposure comes mainly from CO oxidation with O_{ad} atoms. Concerning the effect on morphology change by CO exposure on TiO$_2$, Valden et al.[2] reported that CO exposure at RT had no effect on the morphology of Au(0.25 ML)/TiO$_2$(110), which was observed by STM.

We also measured by MEIS the amounts of ^{18}O for O-TiO$_2$(110) and Au(0.08 ML)/O-TiO$_2$(110) after CO exposure and then dosed with $^{18}O_2$. As clearly seen in Fig. 4 and Fig. 5(b), the amount of adsorbed ^{18}O on Au(0.08 ML)/O-TiO$_2$ exceeds remarkably that on O-TiO$_2$. As can be seen from Fig. 4, the number of eliminated ^{18}O after CO exposure for ^{18}O-TiO$_2$ is quite the same as that adsorbed on O-TiO$_2$ after CO exposure followed by $^{18}O_2$ dose. It must be also noted that no ^{18}O adsorption was observed within the experimental uncertainty for the nearly stoichiometric S^*-TiO$_2$(110) surface after CO exposure followed by $^{18}O_2$ dose. The present UPS and MEIS results demonstrate that the oxidation reaction between O_{ad} and CO is strongly enhanced by Au nano-clusters.

We exposed Au(0.08 ML)/O-TiO$_2$(110) to $^{18}O_2$ (1000 L) at ~325 K - RT and then measured the UPS and MEIS spectra, which are shown in Fig. 6 and Fig. 5(b), respectively. In the UPS measurement, we employed a TiO$_2$(110) substrate with a low

sheet resistance (100 $\Omega/\square$), which has more electronic excess charge than that with a high sheet resistance because of higher density of Ti-int. Except for this case, the sheet resistance of the TiO$_2$(110) supports employed here was ~200 $\Omega/\square$. For such a TiO$_2$ substrate with a low sheet resistance, the defect state intensity for the R-TiO$_2$(110) exposed to O$_2$ still maintains 10 – 20 % of that for the R-TiO$_2$(110) owing to too many subsurface excess charge probably provided by Ti-int. This is explained by the fact that the barrier for O adsorption on the surface increases with increasing the number of O$_{ad}$ from 0.3 up to 0.8 eV, which was predicted by the first principles calculations[17]. As clearly seen, the residual defect state intensity is completely diminished by further O$_2$ exposure onto Au(0.08 ML)/O-TiO$_2$(110), indicating that the residual electronic charge is consumed for further generating O$_{ad}$ atoms. For the Au(0.08 ML)/O-TiO$_2$(110) after exposed to ^{18}O$_2$, the amount of $1.6\pm0.3\times10^{13}$ atoms/cm^2 was additionally adsorbed on the surface, as shown in Fig. 5(b). This additionally adsorbed ^{18}O plus the amount of ^{18}O ($1.8\pm0.3\times10^{13}$ atoms/cm^2) adsorbed on the O-TiO$_2$(110) after CO exposure followed by ^{18}O$_2$ dose almost coincide with that for Au/O-TiO$_2$(110) after CO exposure followed by ^{18}O$_2$ dose (see Fig. 5(b)). This demonstrates that Au nano-clusters lower the potential barrier for the dissociative adsorption of O$_2$ on the TiO$_2$(110) surfaces.

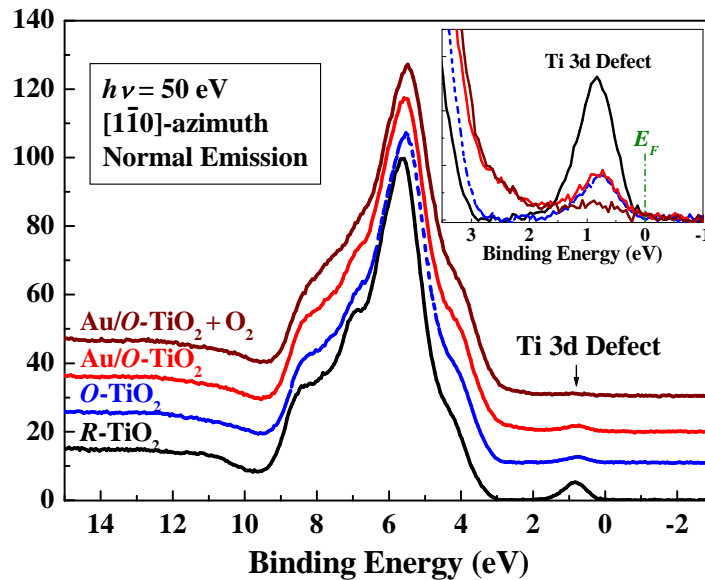Fig. 6. UPS spectra observed for R-, O-TiO$_2$, Au(0.08 ML)/O-TiO$_2$, and Au(0.08 ML)/O-TiO$_2$ after ^{18}O$_2$ exposure of 1000 L at RT. Inset indicates magnified spectra around Ti 3d defect state. Sheet resistance of TiO$_2$ support employed here is ~100 $\Omega/\square$.

C. The mechanism of emerging catalytic activity of Au nano-clusters

The motivation of the present study is to elucidate the mechanism of the emerging activity of Au nano-clusters in the CO oxidation reaction on the $TiO_2(110)$ surfaces. We measured the work functions for the R- and O-$TiO_2(110)$ surfaces deposited with Au nano-clusters. Figure 7 shows the work functions as a function of Au coverage measured by detecting the secondary electron emission induced by 140 eV photon impact on the samples negatively biased. It is clearly seen that the work function drops abruptly by a small amount of Au deposition for O-$TiO_2(110)$, while that for R-$TiO_2(110)$ increases with increasing the Au coverage. This reveals that an electronic charge transfer takes place from Au clusters to O-$TiO_2(110)$ and from R-$TiO_2(110)$ to Au clusters. This result is quite consistent with the theoretical predictions[6,9]. The charge transfer is also seen from the E_B shift of O 2p peak position but not from the valence band edge because of Au 6s band in UPS spectra shown in Fig. 6. The peak position for Au(0.08 ML)/O-TiO_2 is slightly shifted to higher E_B side by ~0.1 eV compared with that for O-TiO_2. Correlated with the above shift, a lower E_B shift of ~0.1 eV was observed for the O 2s line by Au deposition on O-TiO_2(not shown here, see [39]). Importantly, the polarity of the Au/O-TiO_2 interface dipole is opposite to that of O_{ad}/O-TiO_2 because of the electronic charge transfer from Au to O-TiO_2 and of the electro-negativity of O_{ad}. The interaction between the two dipoles with anti-parallel polarity is attractive and thus the Au/O-TiO_2 interface dipole should lower the potential barrier for O adsorption and stabilize the O_{ad} on the 5-fold Ti rows. It is noteworthy that Au nano-clusters grown on the O-$TiO_2(110)$ do not create an electronic excess charge on the surface. Indeed, the defect state intensity does not change after Au(0.08 ML) deposition on the O-$TiO_2(110)$ surface as shown in Fig. 6. Unfortunately, it is impossible to see the binding energy (E_B) shift of the Au 4f line because of the final state effect[40,41] emerging for metal nano-clusters on oxide supports, which leads to apparent higher E_B shifts. The E_B shift of the valence band edge is also intractable because of the Au 6s band. Concerning the enhanced oxidation reaction of CO with O_{ad}, the electric field induced by the interface dipole should play a crucial role. The electric filed polarizes an incoming CO molecule resulting in an attractive interaction between the Au nano-cluster and the polar CO molecule. This effect prolongs the duration time for CO trapped near the perimeter of the Au cluster. With increasing the cluster size, the interface dipoles work effectively only at the perimeter interface

because of the screening by the increased valence electrons, as will be explained later. This situation is consistent with the recent report[12] that the CO oxidation rate normalized by the total number of Au atoms at the perimeter interfaces is constant at 300 K for Au nano-clusters on $TiO_2(110)$.
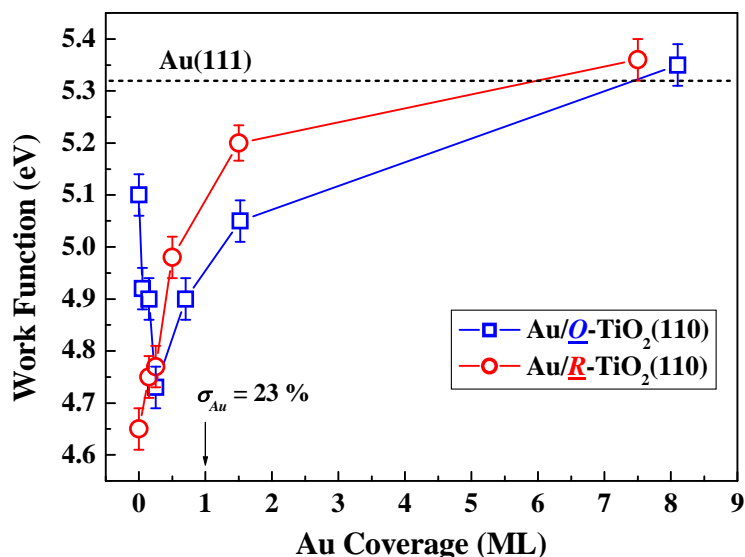

Fig. 7. Work function measured for Au/O-$TiO_2(110)$ (open squares) and Au/R-$TiO_2(110)$ (open circles) as a function of Au coverage. Dashed line indicates the work function of Au(111) (5.31 eV)[38]. Error bars originate from experimental uncertainty of ±0.04 eV.

Finally we analyzed the size-dependent activity of Au nano-clusters. Figure 8 shows the normalized defect state intensity and the reduction of work function compared with that (5.31 eV) for Au(111)[38] after CO exposure of 12000 L, as a function of Au coverage. Obviously, the work function correlates inversely with the normalized defect state intensity. This is quite reasonable, because the electronegative species of O_{ad} increases the work function and CO reacts with the O_{ad} to form CO_2, which escapes from the surface. The present results demonstrate that the optimum Au cluster size is around 0.05 ML, corresponding to 2D clusters with an average diameter of 1.4 nm and two atomic layer height (see Figs, 2(b) and (c)). In this case, the number of Au atoms comprising the cluster is ~50 atoms. This optimum size and shape is consistent with that reported by Valden et al.[2]. In order to confirm that, we measured the amount of ^{18}O by MEIS for Au/O-$TiO_2(110)$ after CO exposure followed by $^{18}O_2$ dose. The amounts of ^{18}O observed for Au coverage of 0.05, 0.08 and 0.7 ML,

respectively are 3.1, 3.2, and less than 0.3×10^{13} atoms/cm^2.   At Au coverage of 0.7 ML, the Au clusters take a 3D shape approximated by a partial sphere with an average diameter of 1.8 and height of 0.9 nm (see Fig. 2(b) and (c)) corresponding to ~90 Au atoms per cluster. With increasing the cluster size from the optimum one, the activity is decreased rapidly.   The reduction of the activity is caused by the decrease in the electric field induced by the dipoles at the Au/O-TiO$_2$(110) interface, which is ascribed to the screening of the field by the valence electrons of Au clusters, whose number increases with increasing the Au cluster size..
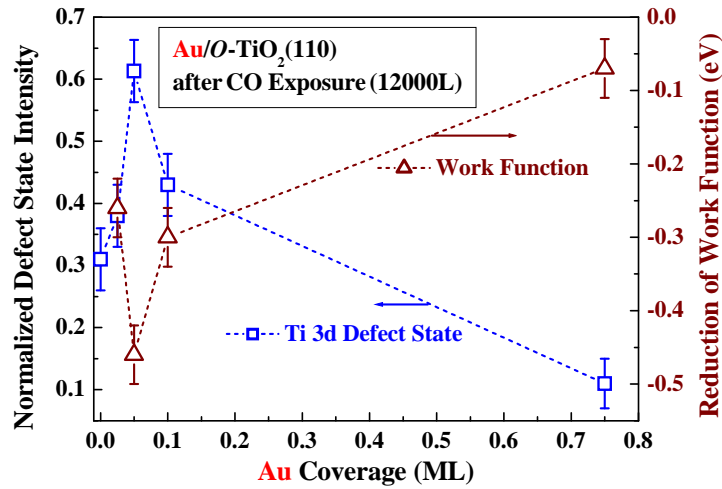

Fig. 8. Defect state intensity (open squares) normalized by that for R-TiO$_2$(110) indicated for Au/O-TiO$_2$(110) after CO exposure of 12000 L as a function of Au coverage.   Right side axis: Reduction of work function (open triangles) relative to that for Au(111) indicated for Au/O-TiO$_2$(110) after CO exposure of 12000 L as a function of Au coverage.

IV. CONCLUSION

We have found a reaction path that CO molecules react with the O$_{ad}$ atoms adsorbed on the 5-fold Ti rows at RT.   This CO oxidation reaction is enhanced pronouncedly by the presence of Au nano-clusters on the O-TiO$_2$(110) surfaces.   The activity does not emerge on nearly stoichiometric TiO$_2$(110) surfaces.   This strong activity is attributed to an electronic charge transfer from Au to the O-TiO$_2$ support to form an interface dipole and not to creation of a surface excess charge like a Ti^{3+} state.   The interface dipole with a polarity of positive charge on the vacuum side which is opposite to the O$_{ad}$ on the 5-fold Ti rows induces an attractive interaction between them and thus lowers the

potential barrier for the dissociative adsorption of O_2 on the 5-fold Ti rows. This interface dipole also generates an attractive force upon a polar CO molecule, which leads to trap of the CO near the perimeter interface of Au/O-TiO_2(110).   This trapping enhances the reaction rate of CO oxidation.   The catalytic activity is strongly dependent on the size and shape of Au nano-clusters. The marked activity appears for 2D clusters with a lateral size of ~1.5 nm and two atomic layer height (~50 Au atoms per cluster) and decreases abruptly with increasing the cluster size.   This indicates that the electric field of the interface dipole is screened by the valence electrons of 3D Au nano-clusters, the larger the cluster size the stronger the screening effect.   The interface dipoles work effectively only at the periphery of Au nano-clusters and thus the oxidation rate is well correlated with the total number of Au atoms located at the perimeter interfaces.

ACKNOWLEDGMENTS

References

[1] M. Haruta, T. Kobayashi, H. Sano, N. Yamada,   Chem. Lett. **2**, 405 (1987).

[2] M. Valden, X. Lai, and D.W. Goodman,   Science **281,** 1647 (1998).

[3] A. Sanchez, S. Abbet, U. Heiz, W.-D. Schneider, H. Häkkinen, R.N. Barnett, and U. Landman,   J. Phys. Chem. **A 103**, 9573 (1999).

[4] F. Boccuzzi, A. Chiorino, M. Manzoli, P. Lu, T. Akita, S. Ichikawa, and M. Haruta, J. Catal. **202**, 256 (2001).

[5] T. Minato, T. Susaki, H.S. Kato, M. Kawai, and K. Aika,   Surf. Sci. **566-568**, 1012 (2004).

[6] J.G. Wang and B. Hammer,   Phys. Rev. Lett. **97**, 136107 (2006).

[7] M.S. Chen and D.W. Goodman,   Catal. Today **111**, 22 (2006).

[8] D. Matthey, J.G. Wang, S. Wendt, J. Matthiesen, R. Schaub, E/ Lægsgaard, B. Hammer and, F. Besenbacher, Science **315**, 1692 (2007).

[9] H. Shi, M. Kohyama, S. Tanaka, and S. Takeda, Phys. Rev. **B 80**, 155413 (2009).

[10] Z.-P. Liu, S.J. Jenkins, and D.A. King, Phys. Rev. Lett. **94**, 196102 (2005).

[11] A. Bongiorno and U. Landman, Phys. Rev. Lett. **95**, 106102 (2005).

[12] T. Fujitani and I. Nakamura, Angew. Chem. Int. Ed. **50**, 10144 (2011).

[13] A. Visikovskiy, H. Matsumoto, K. Mitsuhara, T. Nakada, T. Akita and Y. Kido, Phys. Rev. **B 83**, 165428 (2011).

[14] B. Hammer and J.K. Nørskov, Nature **376**, 238 (1995).

[15] K. Mitsuhara, H. Okumura, A. Visikovskiy, M. Takizawa, and Y. Kido, Chem. Phys. Lett. **513**, 84 (2011).

[16] K. Mitsuhara, T. Matsuda, H. Okumura, A. Visikovskiy, and Y. Kido, Nucl. Instrum. Methods **B 269**, 1859 (2011).

[17] S. Wendt, P.T. Sprunger, E. Lira, G.K.H. Madsen, Z. Li, J.Ø. Hansen, J. Matthiesen, A.B. Rasmussen, E. Lægsgaard, B. Hammer, and F. Besenbacher, Science **320**, 1755 (2008).

[18] P. Krüger, S. Bourgeois, B. Domenichini, H. Magnan, D. Chandesris, P. Le Fèvre, A.M. Flank, J. Jupille, L. Floreano, A. Cossaro, A. Verdini, and A. Morgante, Phys. Rev. Lett. **100**, 055501 (2008).

[19] T. Minato, Y. Sainoo, Y. Kim, H.S. Kato, K. Aika, M. Kawai, J. Zhao, H. Petek, T. Huang, W. He, B. Wang, Z. Wang, Y. Zhao, J. Yang, and J.G. Hou, J. Chem. Phys. **130**, 124502 (2009).

[20] Y. Du, N.A. Deskins, Z. Zhang, Z. Dohnálek, M. Dupuis, and I. Lyubinetsky, Phys. Chem. Chem. Phys. **12**, 6337 (2010).

[21] H. Matsumoto, K. Mitsuhara, A. Visikovskiy, T. Akita, N. Toshima and Y. Kido Nuclear Instruments and Methods **B 268** (2010) 2281-2284.

[22] M. Aono and R.R. Hasiguti, Phys. Rev. **B 48**, 12406 (1993).

[23] M.A. Henderson, Surf. Sci. **419**, 174 (1999).

[24] R.L. Kurtz, R. Stockbauer, T.E. Madey, E. Román, and J.L. de Segovia, Surf. Sci. **218**, 178 (1989).

[25] T. Okazawa, M. Kohyama and Y. Kido, Surf. Sci. **600**, 4430 (2006).

[26] U. Diebold, Surf. Sci. Rep. **48**, 53 (2003).

[27] Y. Kido and T. Koshikawa, J. Appl. Phys. **67**, 187 (1990).

[28] P.L. Grande, A. Hentz, R.P. Pezzi, I.J.R. Baumvol, and G. Schiwietz, Nucl. Instrum. Methods **B 256**, 92 (2007).

[29] M. Hazama, Y. Kitsudo, T. Nishimura, Y. Hoshino, P.L. Grande, G. Schiwietz and Y. Kido, Physical Review **B 78**, 193402 (2008).

[30] E. Wahlström, N. Lopez, R. Schaub, P. Thostrup, A. Rønnau, C. Africh, E. Lægsgaard, J.K. Nørskov, and F. Besenbacher, Phys. Rev. Lett. **90**, 026101 (2003).

[31] A. Iwamoto, T. Okazawa, T. Akita, I. Vickridge, and Y. Kido, Nucl. Instrum. Methods **B 266**, 965 (2008).

[32] C.M. Yim, C.L. Pang, and G. Thornton, Phys. Rev. Lett. **104**, 036806 (2010).

[33] Y. Du, N.A. Deskins, Z. Zhang, Z. Dohnálek, M. Dupuis, and I. Lyubinetsky, Phys. Chem. Chem. Phys. **12**, 6337 (2010).

[34] A.C. Papageorgiou, N.S. Beglitis, C.L. Pang, G. Teobaldi, G. Cabailh, Q. Chen, A.J. Fisher, W.A. Hofer, and G. Thornton, PNAS **107**, 2391 (2010).

[35] Y. Zhao, Z. Wang, X. Cui, T. Huang, B. Wang, Y. Luo, J. Yang, J. Hou, J. Am. Chem. Soc. **131**, 7958 (2009).

[36] Z. Wang, Y. Zhao, X. Cui, S. Tan, A. Zhao, B. Wang, J. Yang, and J.G. Hou, J. Phys. Chem. **C 114**, 18222 (2010).

[37] Y. Du, N.A. Deskins, Z. Zhang, Z. Dohnálek, M. Dupuis, and I. Lyubinetsky, Phys. Rev. Lett. **102**, 096102 (2009).

[38] S. Hünter, *Photoelectron Spectroscopy 3rd ed*. (Springer, Berlin, 2003).

[39] K, Mitsuhara, Y. Kitsudo, H. Matsumoto, A. Visikovskiy, M. Takizawa,
T. Nishimura, T. Akita, and Y. Kido, Surface Science **604**, 547 (2010).

[40] G.K. Wertheim, S.B. DiCenzo, and S.E. Youngquist, Phys. Rev. Lett. **51**, 2310 (1983).

[41] Y. Kitsudo, A. Iwamoto, H. Matsumoto, K, Mitsuhara, T. Nishimura, M. Takizawa,
T. Akita, Y. Maeda, and Y. Kido, Surface Science **603**, 2108 (2009).